Journal of
Marine Science and Engineering

Article

Mega-Ship-Generated Tsunami: A Field Observation in Tampa Bay, Florida

Ping Wang * and Jun Cheng

Coastal Research Laboratory, School of Geosciences, University of South Florida, Tampa, FL 33620, USA; jun@mail.usf.edu
* Correspondence: pwang@usf.edu

Abstract: The displacement of a large amount of water in a moderate-sized estuary by a fast-moving mega-ship can generate tsunami-like waves. Such waves, generated by cruise ships, were observed in Tampa Bay, Florida, USA. Two distinct, long tsunami-like waves were measured, which were associated with the passage of a large cruise ship. The first wave had a period of 5.4 min and a height of 0.40 m near the shoreline. The second wave had a period of 2.5 min and was 0.23 m high. The peak velocity of the onshore flow during the second wave reached 0.65 m/s. The shorter, second wave propagated considerably faster than the first wave in the breaking zone. The measured wave celerity was less than 50% of the calculated values, using the shallow water approximation of the dispersion equation, suggesting that nonlinear effects play an important role. A fundamental similarity among the generation of tsunamis, as induced by mega-ships, landslides or earthquakes, is a process that causes a vertical velocity at the sea surface, where a freely propagating wave is produced. This mega-ship-generated tsunami provides a prototype field laboratory for systematically studying tsunami dynamics, particularly the strong turbulent flows associated with the breaking of a tsunami wave in the nearshore, and tsunami–land interactions. It also provides a realistic demonstration for public education, which is essential for the preparation and management of this unpreventable hazard.

Keywords: long waves; estuary; ship wake; nearshore hydrodynamics; prototype laboratory

check for updates

Citation: Wang, P.; Cheng, J. Mega-Ship-Generated Tsunami: A Field Observation in Tampa Bay, Florida. *J. Mar. Sci. Eng.* **2021**, *9*, 437. https://doi.org/10.3390/jmse9040437

Academic Editor: Claudia Cecioni

Received: 17 February 2021
Accepted: 13 April 2021
Published: 18 April 2021

1. Introduction

Tsunamis are among the deadliest and costliest natural hazards worldwide. The risks can increase significantly in the future, as population density in coastal zones increases and sea-levels rise. The tremendous property damages and fatalities associated with tsunamis are mainly caused by the very strong flow associated with the breaking of the long wave, superimposed on the elevated and fast-rising water level [1,2] (Flow velocities of over 10 m/s, and up to 17 m/s, associated with breaking tsunami waves were estimated by Jaffe and Gelfenbuam [3] based on field observations.

A tsunami is a series of waves generated by a sudden displacement of a large volume of water in the ocean. Common mechanisms inducing sudden large water displacement include earthquakes [4–7] and landslides [8–11]. Tsunamis induced by landslides display a greater variety depending on their origin, compared with earthquakes [9]. The generation mechanisms for landslide-induced tsunamis are more diverse, spanning from impulsive waves due to subaerial landslides hitting the water with high-impact velocities [12] to submerged landslides moving farther at lower speeds [13,14]. The mechanism by which landslides occur also plays a key role in wave features and total energy [15]. Sources range from events of local character to large-volume landslides with substantial regional impact [16]. Owing to the above complications, the nature and hazard posed by landslide tsunamis are not as well understood as those by earthquakes [9].

Because these generating mechanisms are not currently predictable, the exact timing and location of a tsunami cannot be forecasted before the occurrence of the generating events. Therefore, the probability approach is typically used to assess potential tsunamic hazards [17]. Once the initial tsunami is generated, the wave form (i.e., free surface elevation) propagation across the ocean can be computed rather accurately [17–20] (Bellotti et al., 2009). Because of the very short time (from minutes to hours) between the generation of a tsunami and its arrival at the shoreline, public knowledge of tsunami behavior in the nearshore zone is crucial to developing effective response plans in the preparation for this unpreventable natural hazard.

A moving vessel can generate both short and long waves in an estuary. Soomere [21] provided an extensive review of long waves generated by moving ships in semi-enclosed shallow water bodies. Fenical et al. [22] measured a water surface elevation fluctuation of up to 1 m in magnitude and 120 s in period caused by deep-draft vessels in the Corpus Christi Ship Channel, Texas, USA. Didenkulova et al. [23] discussed the potential of using waves generated by fast-moving ferries as a physical model for studying tsunami and found that ship-generated tsunamis would provide an ideal natural laboratory to simulate landslide-induced tsunamis. Grue [24,25] examined the physics underlying the ship-generated tsunamis and suggested that depth change in shallow waters plays an important role in the generation of a tsunami.

In this study, we observed a series of tsunami-like waves generated by mega-ships, cruise ships in this case, in the upper Tampa Bay, Florida, USA. The water level and current were measured using an array of sensors in the nearshore zone where the breaking of the long wave occurred. The purpose of this paper is to provide a case study on the hydrodynamic conditions associated with breaking tsunami waves in the nearshore zone. The field scenario can be used for the systematic measurement of tsunami dynamics and tsunami–land interaction at prototype scales. The rather realistic tsunami-like wave can also be used for public education on tsunami behavior in the nearshore area.

2. Study Area and Methods

Our field measurements were conducted in the Upper Tampa Bay (Figure 1A,B), Florida, USA. The Upper Tampa Bay is approximately 10 km long and 7 km wide (Figure 1C). The 11-m-deep main shipping channel is roughly 2.5 km east of the shoreline where the measurements were conducted. Two large spoil islands are located east of the main channel. Water depth outside the main shipping channel ranges from 2 to 5 m. Shallow water, less than 1 m deep, extends about 200 m from the shoreline where the field measurements were conducted (Figure 1D).

The large cruise ship involved in this study is 294 m long with a 32 m beam width and 7.8 m draft. The ship sails at approximately 15 knots (28 km/h) in front of the study site, displacing a significant amount of water relative to the bay size, and generates tsunami-like waves. This mechanism bears considerable similarity to tsunami generation by a landslide [26,27]. As the long wave propagates toward the shoreline, it shoals and breaks. The present field measurements were focused within the breaker zone (Figure 1D). Two sets of measurement were conducted, one on 9 January 2011 (referred to as the 010911 measurement in the following) and one on 29 January 2011 (the 012911 measurement). The beach profile, as shown in Figure 1D, was surveyed at the beginning of the experiment. Both experiments and the rising and falling of water level were recorded with a video camera.

For the 010911 measurement, three synchronized pressure sensors and current meters (acoustic Doppler velocimeters (ADVs)) were deployed to measure the tsunami wave and the associated currents (Figure 1D). The offshore gauge malfunctioned and did not yield reliable data. The middle sensor was sampling at 2 Hz. The inshore sensor was connected to the shore-based power source and data storage, sampling continuously at a high frequency of 8 Hz. For the 012911 measurement, only the inshore sensor was used with the goal of repeating the 010911 measurement. Similar tsunami waves were measured on 012911. The following discussion focuses on the first measurement with more sensors.

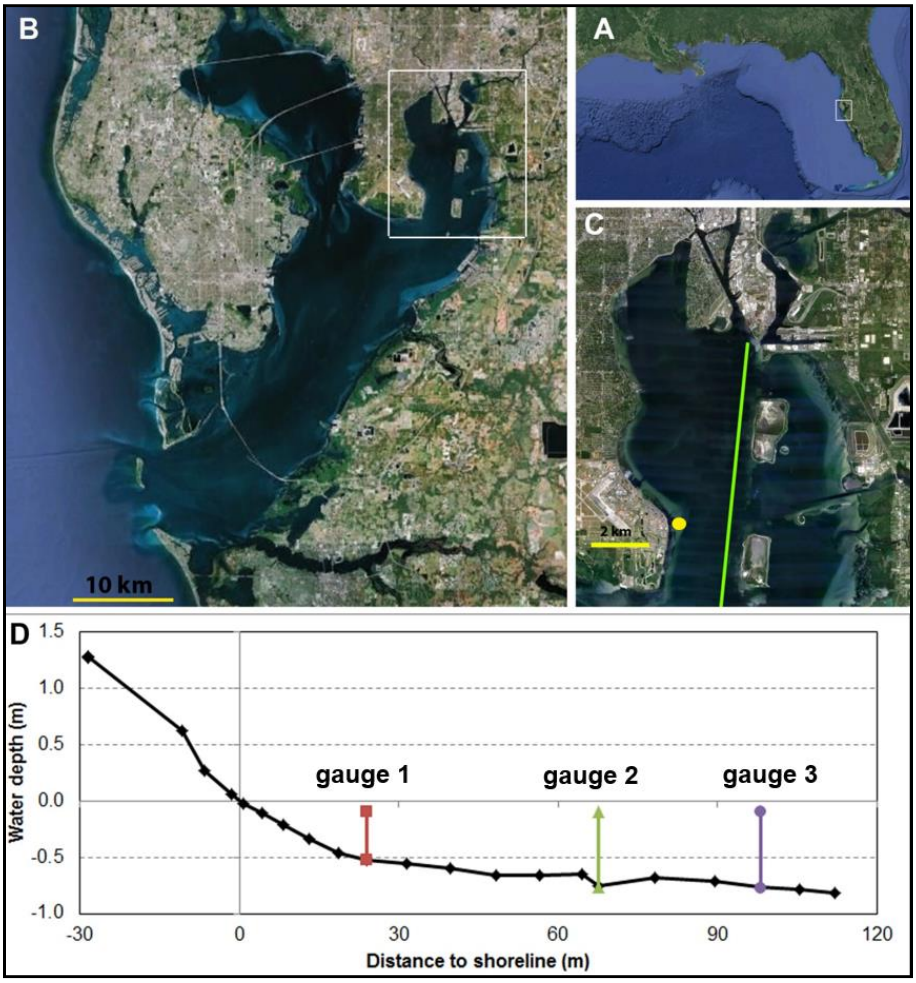

Figure 1. The field study site at Upper Tampa Bay. (**A**) The Southeast US and the Gulf of Mexico coasts. (**B**) Tampa Bay. (**C**) Upper Tampa Bay, illustrating the main shipping channel (green line) and the study site (yellow circle). (**D**) The gentle nearshore profile and locations of the three measurement stations.

Spikes sometimes occur in ADV measurements as caused by the Doppler signal aliasing and/or air bubbles [28]. A 3D phase space method, originally developed by Goring and Nikora [29] and validated by Mori et al. [30], was applied to eliminate the erroneous spikes. The removed data points were replaced using a cubic polynomial curve fitting. The Butterworth low-pass filter (with a half-minute threshold) was applied to the water level and velocity data in order to examine the long tsunami-like wave. The velocity skewness of the two long waves was computed based on Ribberink and Al-Salem [31] as

$$R_u = \frac{U_{max}}{U_{max} - U_{min}} \tag{1}$$

where U_{max} is the maximum value of onshore-directed velocity and U_{min} is the maximum value of offshore-directed velocity during a one wave cycle.

The propagation speed of the tsunami-like wave form can be obtained from the measurements at the two gauges, which were 43.7 m apart (Figure 1). The speed of the wave form was calculated using two methods. For the first method, the travel time was determined based on the arrival of the wave crest at the two gauges. In the second method, the travel time was obtained using a cross-correlation analysis [32], which identified the phase lag between the waves measured at the two gauges. The first method considered only the wave peak, while the second method incorporated the entire wave form. Based on the linear wave theory (Equation (2)) and the Boussinesq approximation of solitary wave theory (Equation (3)), the wave speed in shallow water can be calculated as [33,34]

$$c = \sqrt{gh} \tag{2}$$

$$c = \sqrt{g(h + H)} \tag{3}$$

where c is wave speed, g is gravitational acceleration, h is water depth, and H is wave height. The measured wave speed was compared with the calculated values to investigate the applicability of these commonly used analytical methods.

3. Results

The maximum and minimum values of the free surface elevation time series, induced by the ship-generated tsunami, are shown in Figure 2. The arrival of the high-frequency ship wakes at an oblique angle to the shoreline during the trough of the tsunami-like wave is also illustrated in Figure 2 (lower panel). A large area of the gentle intertidal zone was exposed during the arrival of the trough. The tsunami-like wave crest arrived first. The flooding of the beach at the tsunami peak and the exposure of the intertidal zone at the trough are apparent.

Figure 2. Photos of the ship-generated tsunami. Upper image: shoreline condition before the arrival of the tsunami wave. Middle image: at the peak of the tsunami. Lower image: at the trough of the tsunami.

Figure 3 shows the measured water level, alongshore and cross-shore the current velocities. As expected, onshore flow was measured during the rising phase of the tsunami (Figure 3C), and offshore flow was measured during the retreating phase of the tsunami (Figure 3C). The tsunami wave arrived at an angle to the shoreline, generating both a longshore and cross-shore current.

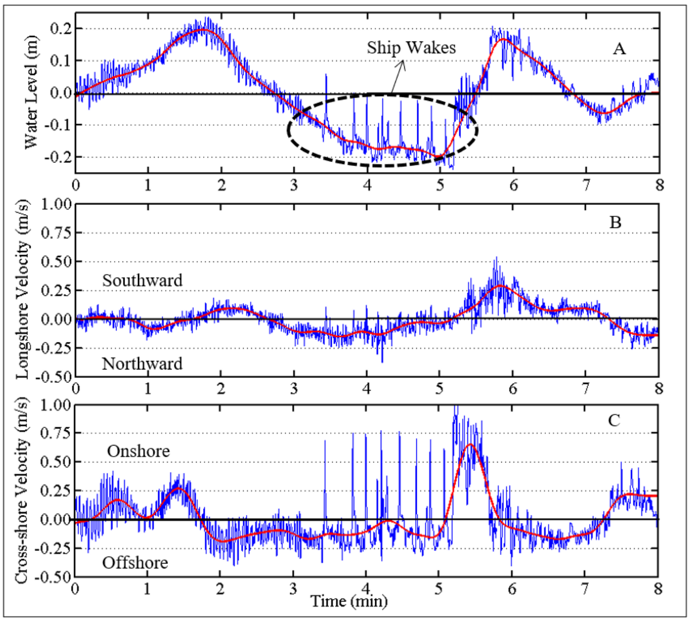

Figure 3. The measured free surface elevation variations and currents at gauge 1 during the passage of two consecutive tsunami waves. Blue lines represent the raw record sampled at 8 Hz. Red lines represent a low-pass filtered record. (**A**) Water-level fluctuation associated with the two tsunami waves. (**B**) Longshore current associated with the tsunami waves. (**C**) Cross-shore current during the two tsunami waves; note the much stronger onshore current during the arrival of the second wave.

Two distinctive tsunami-like waves were captured by the nearshore gauge (Figure 3), located at 24 m from the pre-tsunami shoreline, during the 010911 measurement. Based on the low-pass filtered water-level fluctuations, the first tsunami-like wave had a period of 5.4 min (measured between two consecutive zero water levels) and a wave height of roughly 0.40 m (Figure 3A). The long wave travelled faster and arrived at the shoreline sooner than the high-frequency ship wakes, which arrived with the trough of the tsunami wave in this case. Cross-shore velocity skewness, as calculated from Equation (1) was 0.58 for the first wave, indicating that the peak onshore velocity was greater than the peak offshore velocity: 0.26 m/s versus 0.19 m/s. For the first wave, the rising phase lasted approximately 1.66 min, while the falling phase was 3.31 min, which was nearly 2.0 times longer than the rising phase. It is worth noting that the rising phase of the first wave started at roughly the mean sea level, while the falling phase extended from the peak of the wave to the trough. The wind waves, superimposed on the long wave, had a wave period of roughly 2 s and a wave height of less than 10 cm (Figure 3A).

The second tsunami-like wave had a slightly lower peak water level as compared to the first wave, 0.17 m versus 0.20 m. The trough of the second wave was much higher than that of the first wave: 0.06 m versus 0.20 m relative to the mean water level. These resulted in a lower overall wave height of 0.23 m for the second wave versus the 0.40 m for the first wave. The second tsunami-like wave had a period of 2.5 min, measured between consecutive zero water levels. This is less than half of the 5.4 min for the first wave. The rising phase of the second wave took about 0.89 min, while the falling phase was approximately 1.38 min, which was 1.54 times longer than the rising phase. It is worth noting that the rising phase started at the lower first trough, while the falling phase ended at the higher second trough. The cross-shore velocity skewness (Equation (1)) for the second wave was 0.79, indicating a much greater onshore flow velocity than the offshore flow velocity: 0.65 m/s versus 0.17 m/s. Due to the arrival of the high-frequency ship wakes, the instantaneous velocity reached nearly 1 m/s (Figure 3C) at the peak of the second wave.

The ship wakes arrived about 2 min after the peak of the first long wave. The ship-wake waves were more than two times higher than the small wind waves (Figure 3A). Similar to the long waves, the measured breaking ship wake was also highly skewed, with a narrow peak and a broad trough superimposed by short wind waves (Figure 4). The time interval between the consecutive ship-wake waves ranged from 10 to 20 s. Eight distinctive ship-wake waves were identified from the nearshore measurements. The ship-wake wave period of 10–20 s (Figure 4), determined based on the time interval between consecutive peaks, is much longer than the typical wake waves reported, which are likely controlled by the size of the ship [21–23,35,36].

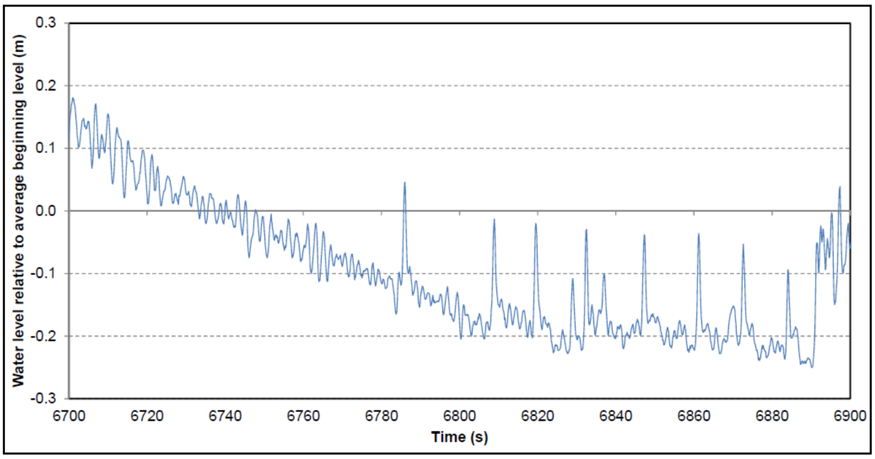

Figure 4. The measured water-level fluctuations associated with the arrival of the ship wakes.

Based on observations during the field measurements, the tsunami-like wave approached the shoreline at an oblique angle. The ship was sailing past the study site from north to south. For the first tsunami-like wave, the longshore current was flowing to the north, opposite to the ship's sailing direction, at the beginning of the rising phase (Figure 3B). The flow direction changed to southward as the water level approached the peak. The southward flow continued as the water level started to subside. The flow direction switched to northward about one-third of the way during the falling phase. The longshore current direction changed again during the rising phase of the second tsunami-like wave. Similar to the case of cross-shore velocity, the strongest longshore current of 0.29 m/s was measured during the passage of the second wave. Stronger currents associated with the second tsunami wave have also been reported based on field observations [37,38]. The second tsunami-like wave also arrived with some of the high-frequency ship wakes, although they were smaller than the major ship wakes that arrived at the previous trough.

4. Discussion

Accurately quantifying the speed of the breaking tsunami wave is important for preparing, managing and assessing this hazard. Based on the dispersion equation, the wave-form speed in shallow waters can be computed using Equations (2) and (3). The computed wave speed was compared with the measured speed in Table 1. The distance between the two gauges was 43.7 m. Based on the cross-correlation analysis of the wave forms measured at gauges 2 and 1, the phase lags, i.e., the travel times, of 59 s and 41 s were obtained for the first and second waves, respectively (Figure 5). This yielded a wave speed of 0.74 m/s for the first wave and 1.07 m/s for the second wave. Based on the arrival time of the peak water level (Figure 6), the first wave was travelling at 0.59 m/s and the second wave at 1.12 m/s. The two methods yielded considerably different wave speeds for the first wave (20%), but similar speeds for the second wave (5%). This is because the shorter, second wave maintained a similar shape at the two measurement locations, while the longer, first wave was deformed.

Table 1. Comparison among measured and calculated wave speeds.

	Measured Cross-Correlation m/s	Measured Arrival of Wave Peak m/s	Calculated Linear Wave m/s	Calculated Solitary Wave m/s
1st wave	0.74	0.59	2.46	3.16
2nd wave	1.07	1.12	2.46	2.91

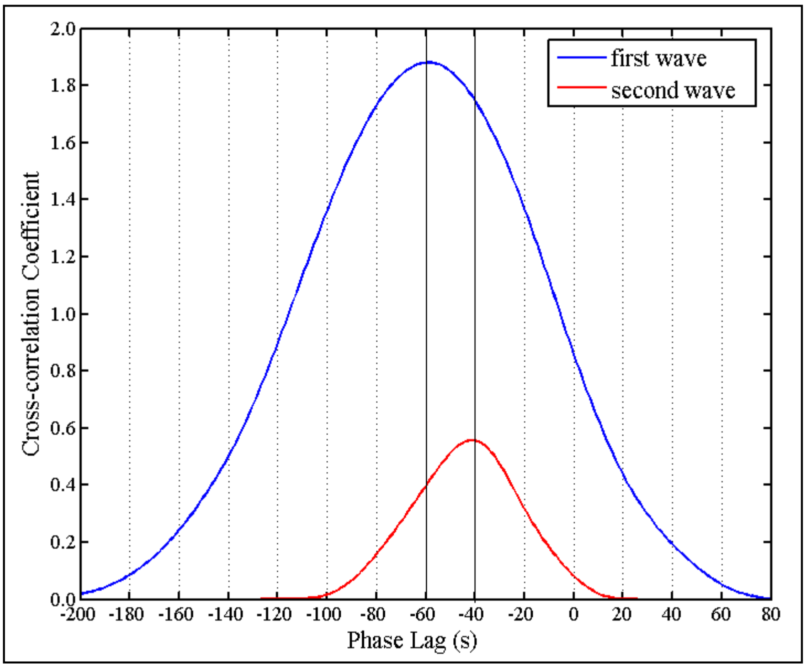

Figure 5. Cross-correlation of the two tsunami-like waves. For the first wave, the maximum cross-correlation coefficient corresponds to a phase shift of 59 s. For the second wave, the maximum cross-correlation coefficient corresponds to a phase shift of 41 s.

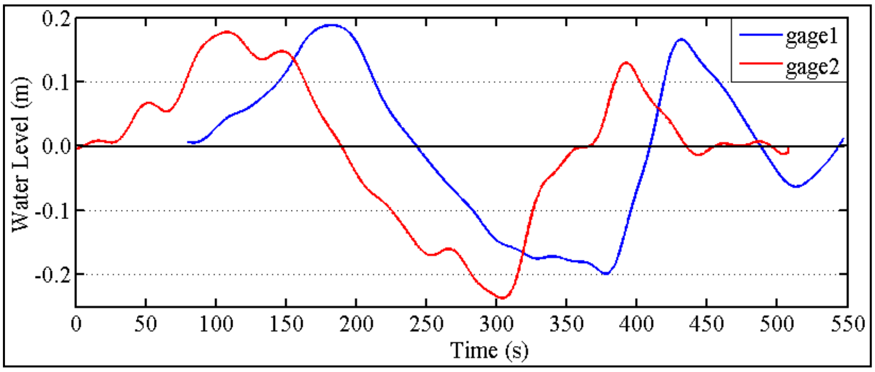

Figure 6. The low-pass filtered long waves measured at the two nearshore locations. The measurement locations are shown in Figure 1D.

The measured wave speeds for both the first and second waves are much slower than the speeds calculated based on the dispersion equation (Table 1). The average water depth between the two measurement locations (Figure 1D) was used in the calculation. The higher order wave theory yielded a greater wave speed. Nonlinear effects were not considered in the shallow water approximation (Equations (2) and (3)) of the dispersion equation. Based on this study, nonlinear effects played a significant role. For the longer, first wave, the measured speed based on the travel time of wave peak is only 24% of the calculated value based on the linear wave theory. For the shorter, second wave, the measured speed is 46% of the calculated value based on the linear wave theory. Thornton and Guza [39] found that the measured wave celerity for typical wind waves compared well, between +20% to −10%, with the linear wave approximation (Equation (2)). For the long waves examined here, Equation (2) over-predicted the wave celerity by more than 100%. Therefore, nonlinear effects should be incorporated.

It is valuable to compare the mechanism of ship-induced tsunamis with those generated by other sources. A considerable amount of research has been conducted on tsunami generations by landslides [8,13,40–42] and earthquakes [5–7,9]. Ship-generated tsunamis can provide a semi-controlled case for the quantification of the breaking of tsunami waves and subsequent interactions with land. Grue [24,25]) derived the tsunami generation by ships. Here, a simplified version of the Grue [25] derivation is applied to qualitatively illustrate a fundamental similarity between the ship-generated tsunamis and those generated by other mechanisms.

Assuming a ship sailing at a constant speed of U, the water depth at time T_1 is h, where the sea bottom is flat. At time T_2, the water depth is reduced to $h/2$ over a sloping bottom (Figure 7). The vertical velocity V_n can be approximated by Equation (4) (simplified from Grue [25]).

$$V_n = -U\frac{d\zeta}{dx}(1 + z/h) \quad (4)$$

where ζ is the shape of the ship bow, and z is the vertical coordinate. At T_1 over the flat bottom (Figure 7, left panel), $z = -h$, and V_n equals to zero (Equation (4)). Thus, over a flat bottom, the ship does not induce a vertical velocity. However, if the ship sails over a sloping bottom (Figure 7, right panel), a vertical velocity is generated (Equation (4)). For example, at depth $z = -h/2$, $V_n = -\frac{1}{2}U\frac{d\zeta}{dx}$ (Figure 7, right panel, blue arrow). Since the flow cannot go through the sea bottom, a reaction velocity with the same magnitude but from an opposite direction occurs (Figure 7, right panel, black arrow). The A_1 velocity appears as a vertical velocity on the ocean's surface at the ship's bow (Figure 7, right panel, red arrow). This vertical velocity creates tsunamis waves in a similar manner as an earthquake or a landslide.

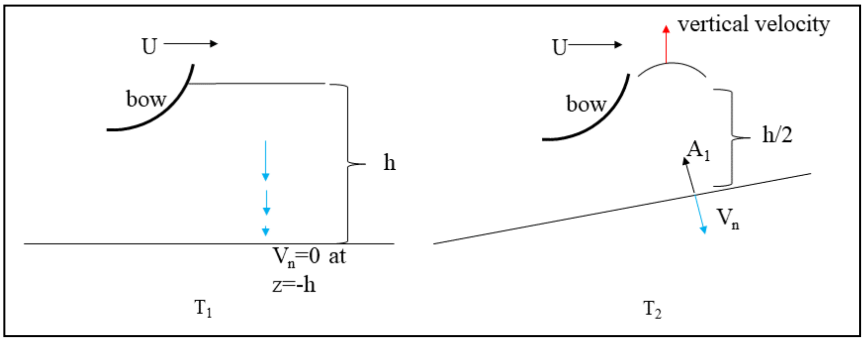

Figure 7. Ship-induced vertical velocity and wave generation at the bow. Left panel indicates time T_1 with a flat bottom. Right panel illustrates time T_2 with sloping bottom

Thus, the generation of tsunami waves by a ship, landslide, or earthquake bears a similar process, which leads to a vertical velocity at the water surface, where a freely propagating wave is produced. The characteristics of the process at the sea bottom controls the features of the tsunami wave at the origin. The temporal and spatial scales during the tsunami generation phase are certainly different among ships, earthquakes, and landslides. However, when the tsunami waves propagate toward the shore, the overall process can be rather similar. For instance, Didenkulova [23] found that many governing nondimensional parameters, such as the Reynolds and Ursell numbers, and the surf-similarity parameters of large-ship waves and landslide tsunamis, are all of the same order of magnitude.

The above similarity between ship-generated tsunamis and those induced by other sources, i.e., landslides and earthquakes, provides a solid scientific basis for the application of ship-generated tsunamis, to help understand natural tsunamis. Given the easy and manageable field conditions in harbors and estuaries, as well as the typically regular ship sailing schedule, ship-generated tsunamis can provide a prototype field laboratory for the quantification of the breaking of tsunami waves and tsunami–land interactions.

5. Conclusions

The long waves generated by a fast-moving large cruise ship (at 28 km/h) in an estuary (Upper Tampa Bay) bear significant similarities to tsunami waves and can be used as a prototype, physical model for systematic studies on the breaking of tsunami waves and tsunami–land interactions. Two distinct, long tsunami-like waves associated with the passage of the cruise ship were measured. The first wave had a period of 5.4 min and a height of 0.40 m near the shoreline. The second wave was 0.23 m high with a period of 2.5 min, generating the strongest onshore flow of 0.65 m/s. Both waves were skewed onshore with shorter and, therefore, faster, rising phases and longer falling phases, corresponding with stronger onshore flow than offshore flow, characteristic of a breaking wave. The measured wave celerity was less than 50% of the calculated values using the shallow water approximation of the dispersion equation, suggesting that nonlinear effects play an important role. The shorter, second wave propagated considerably faster than the first wave in the breaking zone. This mega-ship-generated tsunami provides a prototype field laboratory for systematically studying tsunami dynamics, particularly the strong turbulent flows associated with breaking tsunami waves in the nearshore, and tsunami–land interaction.

Author Contributions: P.W.: Conceptualization, Methodology, Most data analysis, Leading writing. J.C.: Conceptualization, Methodology, Some data analysis, Writing. All authors have read and agreed to the published version of the manuscript.

Funding: This research received no external funding.

Institutional Review Board Statement: Not applicable.

Informed Consent Statement: Not applicable.

Data Availability Statement: The data will be made available upon request to the authors.

Acknowledgments: We are grateful to the two anonymous reviewers and the editor for their constructive comments and suggestions, which improved the original manuscript. We thank John Grue from the University of Oslo for the helpful discussions on the physics of ship-generated tsunamis.

Conflicts of Interest: The authors declare that they have no conflict of interest

References

1. Liu, P.L.-F.; Lynett, P.; Fernando, H.; Jaffe, B.E.; Fritz, H.; Higman, B.; Morton, R.; Goff, J.; Synolakis, C. Observations by the international tsunami survey team in Sri Lanka. *Science* **2005**, *308*, 1595. [CrossRef]
2. Lynett, P.J. Observations and modeling of tsunami-induced currents in ports and harbors. *Earth Planet. Sci. Lett.* **2012**, *327–328*, 68–74. [CrossRef]
3. Jaffe, B.E.; Gelfenbaum, G.A. A simple model for calculating tsunami flow speed from tsunami deposits. *Sediment. Geol.* **2007**, *200*, 347–361. [CrossRef]
4. Moore, G.F.; Bangs, N.L.; Taira, A.; Kuramoto, S.; Pangborn, E.; Tobin, H.J. Three-dimensional splay fault geometry and implications for tsunami generation. *Science* **2007**, 1128–1131. [CrossRef]
5. Fujii, Y.; Satake, K.; Sakai, S.; Shinohara, M.; Kanazawa, T. Tsunami source of the 2011 off the Pacific coast of Tohoku Earthquake. *Earth Planets Space* **2011**, *63*. [CrossRef]
6. Maeda, K.; Furumura, T.; Sakai, S.; Shinohara, M. Significant tsunami observed at ocean-bottom pressure gauges during the 2011 off the Pacific coast of Tohoku Earthquake. *Earth Planets Space* **2011**, *63*, 803–808. [CrossRef]
7. Davis, G. Tsunami variability from uncalibrated stochastic earthquake models: Tests against deep ocean observations 2006–2016. *Geophys. J. Int.* **2019**, *218*, 3. [CrossRef]
8. Cecioni, C.; Romano, A.; Bellotti, G.; Di Risio, M.; De Girolamo, P. Real—Time inversion of tsunamis generated by landslides. *Nat. Hazards Earth Syst. Sci.* **2011**, *11*, 2511–2520. [CrossRef]

9. Løvholt, F.; Pedersen, G.; Harbitz, C.B.; Glimsdal, S.; Kim, J. On the characteristics of landslide tsunamis. *Philos. Trans. Royal Soc. A Math. Phys. Eng. Sci.* **2015**, *373*, 20140376. [CrossRef] [PubMed]
10. Bellotti, G.; Romano, A. Wavenumber—Frequency analysis of landslide—Generated tsunamis at a conical island. Part II: EOF and modal analysis. *Coast. Eng.* **2017**, *128*, 84–91. [CrossRef]
11. Ruffini, G.; Heller, V.; Briganti, R. Numerical modelling of landslide—Tsunami propagation in a wide range of idealised water body geometries. *Coast. Eng.* **2019**, *153*, 103518. [CrossRef]
12. Heidarzadeh, M.; Ishibe, T.; Sandanbata, O.; Muhari, A.; Wijanarto, A.B. Numerical modeling of the subaerial landslide source of the 22 December 2018 Anak Krakatoa volcanic tsunami. Indonesia. *Ocean Eng.* **2020**, *195*, 106733. [CrossRef]
13. Enet, F.; Grilli, S.T. Experimental study of tsunami generation by three—Dimensional rigid underwater landslides. *J. Waterw. Port. Coast. Ocean. Eng. ASCE* **2007**, *133*, 442–454. [CrossRef]
14. Romano, A.; Lara, J.; Barajas, G.; Di Paolo, B.; Bellotti, G.; Di Risio, M.; Losada, I.J.; De Girolamo, P. Tsunamis generated by submerged landslides: Numerical analysis of the near-field wave characteristics. *J. Geophys. Res. Oceans* **2020**, *125*, 125. [CrossRef]
15. Abadie, S.; Harris, J.; Grilli, S.; Fabre, R. Numerical modeling of tsunami waves generated by the flank collapse of the Cumbre Vieja Volcano (La Palma, Canary Islands): Tsunami source and near field effects. *J. Geophys. Res.* **2012**, *117*, C05030. [CrossRef]
16. Koh, H.L.; Tan, W.K.; Teh, S.Y.; Chai, M.F. Simulation of potentially catastrophic landslide tsunami in North West Borneo Trough. *Int. J. Environ. Sci. Dev.* **2016**, *7*, 889–895. [CrossRef]
17. Gonzalez, F.I.; Geist, E.L.; Jaffe, B.; Kanoglu, U.; Mofjeld, H.; Synolakis, C.E.; Titov, V.V.; Arcas, D.; Bellomo, D.; Carlton, D.; et al. Probabilistic tsunami hazard assessment at seaside, Oregon for near- and far-field seismic sources. *J. Geophys. Res.* **2009**, *114*, 11023. [CrossRef]
18. Titov, V.V.; Gonzalez, F.I.; Bernard, E.N.; Eble, M.C.; Mofjeld, H.O.; Newman, J.C.; Venturato, A.J. Real-time tsunami forecasting: Challenges and solutions. *Nat. Hazards* **2005**, *35*, 35–41. [CrossRef]
19. Synolakis, C.E.; Bernard, E.N.; Titov, V.V.; Kanoglu, U.; Gonzalez, F. Validation and verification of tsunami numerical models. *Pure Appl. Geophys.* **2008**, *165*, 2197–2228. [CrossRef]
20. Bellotti, G.; Di Risio, M.; De Girolamo, P. Feasibility of tsunami early warning systems for small volcanic islands. *Nat. Hazards Earth Syst. Sci.* **2009**, *9*, 1911–1919. [CrossRef]
21. Soomere, T. Long ship waves in shallow water bodies. In *Applied Wave Mathematics*; Quak, E., Soomere, T., Eds.; Springer: Berlin/Heidelberg, Germany, 2009; pp. 193–228.
22. Fenical, S.; Bermudez, H.; Shepsis, V.; Krams, D.; Carangelo, P. Vessel-generated long-wave measurement and prediction in Corpus Christi Ship Channel, TX. In Proceedings of the Ocean. Wave Measurement and Analysis, San Francisco, CA, USA, 2–6 September 2001; ASCE Press: New York, NY, USA, 2001; pp. 1634–1643.
23. Didenkulova, I.; Pelinovsky, E.; Soomere, T. Can the waves generated by fast ferries be a physical model of tsunami? *Pure Appl. Geophys.* **2011**, *168*, 2071–2082. [CrossRef]
24. Grue, J. Mini-Tsunami made by ship moving across a depth change. *J. Waterw. Port. Coast. Ocean Eng.* **2020**, *146*. [CrossRef]
25. Grue, J. Ship generated mini-tsunamis. *J. Fluid Mech.* **2017**, *816*, 142–166. [CrossRef]
26. Masson, D.G.; Harbitz, C.B.; Wynn, R.B.; Pedersen, G.; Lovholt, F. Submarine landslides: Processes, triggers and hazard prediction. *Phil. Trans. R. Soc. A.* **2006**, *364*, 2009–2039. [CrossRef]
27. Harbitz, C.B.; Lovholt, F.; Pedersen, G.; Masson, D.G. Mechanisms of tsunami generation by submarine landslides: A short review. *Nor. J. Geol.* **2006**, *86*, 255–264.
28. Voulgaris, G.; Trowbridge, J.H. Evaluation of the acoustic Doppler velocimeter (ADV) for turbulence measurements. *J. Atmos. Ocean Technol.* **1998**, *15*, 272–289. [CrossRef]
29. Goring, D.G.; Nikora, V.I. Despiking acoustic Doppler velocimeter data. *J. Hydraul. Eng.* **2002**, *128*, 117–126. [CrossRef]
30. Mori, N.; Suzuki, T.; Kakuno, S. Noise of acoustic Doppler velocimeter data in bubbly flows. *J. Eng. Mech.* **2007**, *133*, 122–125. [CrossRef]
31. Ribberink, J.S.; Al-Salem, A.A. Sediment transport in oscillatory boundary layers in cases of rippled beds and sheet flow. *J. Geophys. Res.* **1994**, *99*, 12707–12727. [CrossRef]
32. Power, H.E.; Hughes, M.G.; Baldock, T.E. A novel method for tracking individual waves in the surf zone. *Coast. Eng.* **2015**, *98*, 26–30. [CrossRef]
33. Dean, R.G.; Dalrymple, R.A. *Water Wave Mechanics for Engineers and Scientists*; Prentice-Hall, Inc.: New Jersey, NJ, USA, 1984; p. 353.
34. Munk, W.H. The solitary wave theory and its applications to surf problems. *Ann. N. Y. Acad. Sci.* **1949**, *51*, 376–424. [CrossRef]
35. Gharbi, S.; Valkov, G.; Hamdi, S.; Nistor, I. Numerical and field study of ship-induced waves along the St. Lawrence waterway, Canada. *Nat. Hazards* **2010**, *54*, 605–621. [CrossRef]
36. Kurennoy, D.; Soomere, T.; Parnell, K.E. Variability in the properties of wakes generated by high-speed ferries. *J. Coast. Res.* **2009**, *56*, 519–523.
37. Papadopoulos, G.; Caputo, R.; Mcadoo, B.; Pavlides, S.; Karatathis, V.; Fokaefs, A.; Orfanogiannaki, K.; Valkaniotis, S. The large tsunami of 26 December 2004: Field observations and eyewitnesses accounts from Sri Lanka, Maldives Is. and Thailand. *Earth Planets Space* **2006**, *58*, 233–241. [CrossRef]
38. Choowong, M.; Murakoshi, N.; Hisada, K.; Charusiri, P.; Charoentitirat, T.; Chutakositkanon, V.; Jankaew, K.; Kanjanapayont, P.; Phantuwongraj, S. 2004 Indian Ocean tsunami inflow and outflow at Phuket, Thailand. *Mar. Geo.* **2008**, *248*, 179–192. [CrossRef]

39. Thornton, E.B.; Guza, R.T. Energy saturation and phase speeds measured on a natural beach. *J. Geophys. Res.* **1982**, *87*, 9499–9508. [CrossRef]
40. Miller, G.; Take, W.A.; Mulligan, R.P.; McDougall, S. Tsunamis generated by long and thin granular landslides in a large flume. *J. Geophys. Res. Ocean* **2017**, *122*, 653–668. [CrossRef]
41. Grilli, S.T.; Tappin, D.R.; Carey, S.; Watt, S.F.; Ward, S.N.; Grilli, A.R.; Engwell, S.L.; Zhang, C.; Kirby, J.T.; Schambach, L.; et al. Modelling of the tsunami from the December 22, 2018 lateral collapse of Anak Krakatau volcano in the Sunda Straits, Indonesia. *Sci. Rep.* **2019**, *9*, 946. [CrossRef]
42. Kim, J.; Løvholt, F.; Issler, D.; Forsberg, C.F. Landslide material control on tsunami genesis—The Storegga slide and tsunami (8100 years BP). *J. Geophys. Res. Oceans* **2019**, *24*, 3607–3627. [CrossRef]